arXiv:0705.0064v1 [cond-mat.other] 1 May 2007

Bright solitary waves and trapped solutions in Bose-Einstein condensates with attractive interactions.

N.G. Parker[1], S. L. Cornish[2], C. S. Adams[2] and A. M. Martin[1]

[1] School of Physics, University of Melbourne, Parkville, Victoria 3010, Australia

[2] Department of Physics, Durham University, Durham, DH1 3LE, UK

Abstract. We analyse the static solutions of attractive Bose-Einstein condensates under transverse confinement, both with and without axial confinement. By full numerical solution of the Gross-Pitaevskii equation and variational methods we map out the condensate solutions, their energetic properties, and their critical points for instability. With no axial confinement a bright solitary wave solution will tend to decay by dispersion unless the interaction energy is close to the critical value for collapse. In contrast, with axial confinement the only decay mechanism is collapse. The stability of a bright solitary wave solution increases with higher radial confinement. Finally we consider the stability of dynamical states containing up to four solitons and find good agreement with recent experiments.

The presence of attractive interactions in Bose-Einstein condensates (BECs) leads to rich and intriguing nonlinear phenomena. A key example is the formation of bright soliton-like structures [1, 2, 3]. A bright soliton is a one-dimensional (1D) density wave that propagates without spreading due to a balance between attractive interactions and dispersion. In 3D and under transverse confinement, the analog is a bright solitary wave (BSW) solution, which is self-trapped in the axial direction [4, 5, 6, 7]. Due to their self-trapped nature, BSWs hold significant advantages for atom-optical applications, such as atom interferometry. Another important property of attractive BECs in 3D is the collapse instability. In 3D a homogeneous condensate with attractive interactions is always unstable to collapse [8]. However, the presence of trapping can stabilise the condensate against collapse up to a critical number of atoms [9, 10]. Indeed, the collapse instability has been crucial in the experimental formation of BSWs [1, 2, 3]. A highly-populated repulsively-interacting BEC has its interactions switched to attractive via a Feshbach resonance. This induces the collapse of the condensate, with one [2] or more [1, 3] BSWs emerging from the collapse. For the case of multiple BSWs, a π-phase difference leads to a repulsive solitonic interaction that is important in stabilising their collisions against collapse [7, 11, 12, 13].

Table 1 summarises the three experiments to date that have generated BSWs of attractive BECs, at Rice University [1], ENS in Paris [2], and JILA [3]. They feature cylindrically-symmetric traps with radial harmonic confinement of frequency ω_r, and either a confining or expulsive axial harmonic potential. Note that due to the presence of axial confinement these are not true solitonic states and from now on we will generally define BSWs to be solutions under zero axial confinement. The strength of the atomic interactions, characterised by the s-wave scattering length a_s ($a_\mathrm{s} < 0$ for attractive interactions), relative to the trapping potential is crucial in determining the onset of collapse, and can be parameterised in terms of the dimensionless parameter [14],

$$k = \frac{N|a_\mathrm{s}|}{a_r}, \tag{1}$$

where $a_r = \sqrt{\hbar/m\omega_r}$ is the radial harmonic oscillator length and m is the atomic mass. Collapse occurs when the atom number N exceeds a critical population N_c or, correspondingly, when the interaction parameter k exceeds a critical value k_c. The

Table 1. Parameters of the three matter wave 'solitons' experiments to date. For the ENS experiment, we use an estimated atom number of $N = 4500$, which falls within the error of their measurements, while for the JILA experiment we assume N=1500. The trap ratio λ is defined as $\lambda = \omega_z/\omega_r$.

Experiment	Atomic species	$\omega_r/2\pi$ (Hz)	$\lvert\lambda\rvert$	a_s (nm)	N	k
Rice [1]	^{7}Li	800	0.005 (confining)	-0.16	5000	0.6
ENS [2]	^{7}Li	710	0.1 (expulsive)	-0.21	4500	0.65
JILA [3]	^{85}Rb	17.5	0.4 (confining)	-0.6	1500	0.35

value of k_c is a crucial consideration and has been the subject of several theoretical investigations, both for condensates under a 3D potential [4, 11, 15, 16, 17, 18, 19] and for true BSWs under zero axial confinement [6, 7]. It depends on the geometry of the trap and is of the order of unity. An accurate method to probe k_c is to numerically solve the full 3D Gross-Pitaevskii equation that describes the BEC mean-field, and isolate the point where solutions no longer exist [6, 15, 17, 18]. This method is numerically-intensive but can be approximated using a variational approach [4, 6]. Indeed, the variational method has been used to analyse solutions over the full range of axial trap geometries - confining, expulsive and zero axial trapping. However, this has not been directly compared with the more accurate method of solving the full Gross-Pitaevskii equation. In addition to these methods, the nonpolynomial Gross-Pitaevskii equation, an effective 1D equation derived from the 3D Gross-Pitaevskii equation, has been used to predict the critical interaction parameter for a bright solitary wave [7], while a simple analytic approach [19] has been used to derive the critical interaction parameter for an attractive condensate under 3D trapping.

In this paper we theoretically analyse the solutions of an attractive BEC featuring radial confinement and under the full range of axial potentials - no axial trapping, confining axial potential and expulsive axial potential. This is performed by solving the full Gross-Pitaevskii equation and employing an approximate variational approach. We map the regimes of instability and the energetics of the solutions. In Section 1 we present our theoretical framework of the Gross-Pitaevskii equation and the variational approach. In Section 2 we use these methods to examine the stable BSW solutions in the absence of axial trapping and the occurrence of a finite excitation energy to the solution. In Section 3 we consider the solutions under an axial potential, which is either confining or expulsive, and compare to experiment. Finally in Section 4 we model the multiple interacting 'solitons' observed in the JILA experiment [3] and probe the critical number for such states, finding good agreement between experiment and theory.

1. Theoretical framework

1.1. Gross-Pitaevskii equation

In the limit of zero temperature a dilute BEC can be approximated by a mean-field 'wavefunction' $\psi(\mathbf{r},t)$ which satisfies the Gross-Pitaevskii equation [20],

$$i\hbar\frac{\partial\psi}{\partial t}=\left[-\frac{\hbar^2}{2m}\nabla^2+\frac{1}{2}m\omega_r^2\left(r^2+\lambda^2z^2\right)+gN|\psi|^2\right]\psi. \tag{2}$$

Here N is the number of atoms in the condensate and $g=4\pi\hbar^2a_s/m$ parameterises the strength of the s-wave atomic interactions. The trap used to confine the BEC is assumed to be harmonic and cylindrically-symmetric, where ω_r is the transverse trap frequency and $\lambda=\omega_z/\omega_r$ is the trap ratio. The wavefunction has been normalised such that $\int|\psi(\mathbf{r})|^2d^3\mathbf{r}=1$. Furthermore the energy of the system is defined by the

Gross-Pitaevskii energy functional,

$$E[\psi] = \int d^3\mathbf{r} \left\{ \frac{\hbar^2}{2m}|\nabla\psi(\mathbf{r})|^2 + \frac{1}{2}m\omega_r^2\left(r^2+\lambda^2 z^2\right)|\psi(\mathbf{r})|^2 + \frac{gN}{2}|\psi(\mathbf{r})|^4 \right\} \quad (3)$$

The basic Gross-Pitaevskii equation provides an excellent model of BECs at the mean-field level [21], and although it is insufficient to describe collapse dynamics, where higher order effects such as three-body loss become considerable, it provides a good model to infer the *onset* of collapse [15, 17]. For finite g there are no analytic solutions of the 3D Gross-Pitaevskii equation and we obtain the solutions numerically via the imaginary-time technique: by propagating the Gross-Pitaevskii equation in imaginary time ($t \to -it$), the system relaxes to the lowest energy state of the system [21].

1.2. Variational method

As well as solving the Gross-Pitaevskii equation numerically we use a variational technique to derive approximate solutions and give valuable insight without intensive numerics. Assuming tight radial trapping we decouple the 3D wavefunction $\psi(\mathbf{r})$ into the product of an axial and radial component, with the radial component assumed to be a gaussian harmonic oscillator state [4, 5, 6, 7]. For the axial component there are two regimes:

(i) For $|\lambda| \ll 1$ the axial direction is dominated by interactions. In 1D and the limiting case of $\lambda = 0$, the Gross-Pitaevskii equation supports bright soliton solutions of the form $\psi(z) = \sqrt{2\xi}\mathrm{sech}(z/\xi)$ [20]. The healing length $\xi = \hbar/\sqrt{n_{1\mathrm{D}}m|g|}$ characterises the soliton width, where $n_{1\mathrm{D}}$ is the peak 1D density. Assuming our 3D solution to have this axial profile leads to the ansatz [5, 6, 7],

$$\psi_{\mathrm{sech}}(r,z) = \left(\frac{1}{2\pi l_z l_r^2}\right)^{1/2} \mathrm{sech}\left(\frac{z}{l_z}\right) \exp\left(-\frac{r^2}{2l_r^2}\right). \quad (4)$$

where l_z and l_r represent the axial and radial sizes, respectively. Substituting this ansatz into the energy functional of equation (3) leads to the ansatz energy [6],

$$E_{\mathrm{sech}} = \frac{\hbar^2}{2m}\left(\frac{1}{l_r^2}+\frac{1}{3l_z^2}\right) + \frac{1}{2}m\omega_r^2\left(l_r^2+\frac{\pi^2\lambda^2 l_z^2}{12}\right) + \frac{a_{\mathrm{s}}N\hbar^2}{3ml_z l_r^2}. \quad (5)$$

(ii) For $|\lambda| > 1$, the harmonic potential will dominate the axial direction. For a confining axial potential ($\lambda^2 > 0$), it is then more appropriate to assume a gaussian axial profile. This leads to,

$$\psi_{\mathrm{gaus}}(r,z) = \left(\frac{1}{\pi^{3/2} l_z l_r^2}\right)^{1/2} \exp\left(-\frac{z^2}{2l_z^2}\right) \exp\left(-\frac{r^2}{2l_r^2}\right), \quad (6)$$

and,

$$E_{\mathrm{gaus}} = \frac{\hbar^2}{2m}\left(\frac{1}{l_r^2}+\frac{1}{3l_z^2}\right) + \frac{1}{2}m\omega_r^2\left(l_r^2+\frac{\lambda^2 l_z^2}{2}\right) + \frac{a_{\mathrm{s}}N\hbar^2}{\sqrt{2\pi}ml_z l_r^2}. \quad (7)$$

Equations (5) and (7) define an energy landscape in terms of l_z and l_r. Minimising the energy with respect to these variational parameters leads to the variational solution.

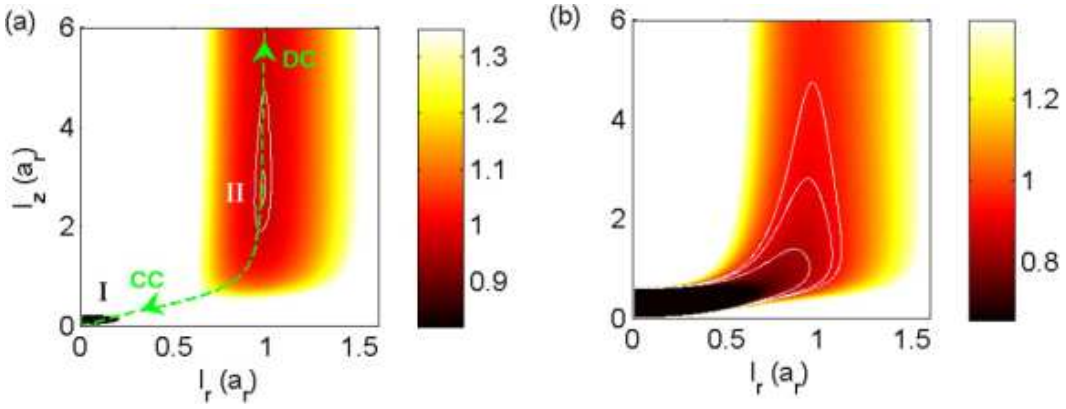

Figure 1. Energy landscape according to equation (5) for $\lambda = 0$ in the (a) stable regime $k < k_c$ ($k = 0.35$) and (b) unstable regime $k > k_c$ ($k = 0.9$). Energy is in units of $\hbar\omega_r$. White contours highlight the shape of the landscapes. In (a) two key regions are indicated: (I) the global energy minimum (collapse region) and (II) the local energy minimum corresponding to the variational solution. Whereas (a) features two minima, corresponding to collapse and the BSW solution, (b) features only a single minima representing collapse. In (a) the dashed green line indicates the low-energy path through the energy landscape from the origin to large l_z. For $l_z < l_z^0$ this path represents the collapse channel (CC) and for $l_z > l_z^0$ it represents the dispersive channel (DC).

2. Bright solitary wave solutions in the absence of axial trapping

2.1. Stable and unstable energy landscapes

We first examine BSW solutions (in the absence of axial trapping) using the variational ansatz of equation (4). This approach been performed previously by Carr and Castin [6], while Perez-Garcia *et al.* [4] performed a similar analysis using the gaussian ansatz of equation (6). A typical energy landscape according to equation (5) for a stable BSW solution is shown in figure 1(a), corresponding to $k = 0.35$. At the origin (region I) the interaction term in equation (5) diverges to negative values since $a_s < 0$ for attractive condensates. This region represents the physical collapse of a wavepacket, although the global energy minimum itself is unphysical since it has zero width ‡. Importantly, there exists a stable local energy minimum indicated by region II in figure 1(a). This represents the BSW solution. A typical unstable energy landscape is shown in figure 1(b), for a large interaction parameter of $k = 0.9$. No local energy minimum exists, and the whole parameter space is unstable to collapse.

2.2. Critical point for collapse

Using the sech-based ansatz of equation (4), Carr and Castin have shown that the critical interaction strength for collapse of a BSW is $k_c^V = 0.76$ [6]. Similarly, Perez-Garcia *et*

‡ In reality the collapse stops at a finite width when the three-body losses become considerable and reduce the atom number to below the critical number [21].

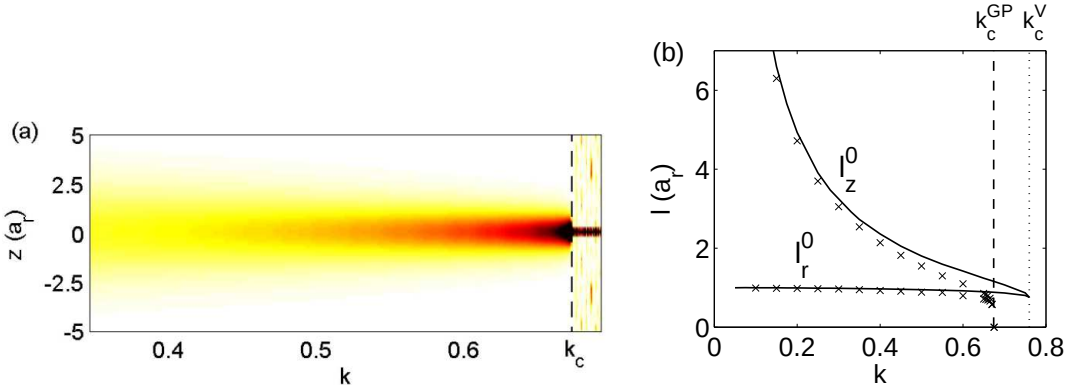

Figure 2. (a) Evolution of the axial density (integrated over the radial direction) of a BSW as the interaction parameter k is adiabatically increased past the critical point for collapse $k_{\rm c}$. The ramping rate is $dk/dt = 0.12$ s^{-1}. (b) Axial and radial width of the BSW as a function of interaction strength k according to the 3D Gross-Pitaevskii equation (crosses) as it evolves under adiabatic ramping. The predictions from the sech-based variational method of equations (4) and (5) are shown by solid lines. The critical interaction strength for collapse according to the sech-based variational method $k_{\rm c}^{\rm V}$ and the Gross-Pitaevskii equation $k_{\rm c}^{\rm GP}$ are indicated by vertical dotted and dashed lines, respectively.

al. [4] have used the gaussian-based ansatz of equation (6) to predict a critical point of $k_{\rm c}^{\rm V} = 0.778$. Using the non-polynomial Gross-Pitaevskii equation, Salasnich *et al.* predict that $k_{\rm c}^{\rm V} = 2/3$ [7]. These methods consider approximated solutions to the 3D Gross-Pitaevskii equation. A more exact method, although considerably more intensive, is to numerically solve the full 3D Gross-Pitaevskii equation [6, 17].

In order to isolate $k_{\rm c}$ from the full 3D Gross-Pitaevskii equation we employ an adiabatic ramping technique. Firstly, a stable BSW solution ($k \ll k_{\rm c}$) is obtained by propagating the 3D Gross-Pitaevskii equation in imaginary time. Then, in real time, the interaction parameter k is increased adiabatically. We employ a ramping rate $dk/dt = 0.12$ s^{-1}. We have verified that a lower ramping rate does not change the point of collapse. An example of a BSW under adiabatic ramping is shown in figure 2(a). For $k < k_{\rm c}$ the condensate progresses through the stationary state solutions, becoming progressively narrower and of higher density, but at $k = k_{\rm c}$ the condensate suddenly collapses. Using this technique we have isolated the critical interaction strength according to the full Gross-Pitaevskii equation for a BSW to be $k_{\rm c}^{\rm GP} = (0.675 \pm 0.005)$. The error margin arises from the finite time over which the wavepacket collapses. We have confirmed that if the value of k is ramped up to, and then maintained at, any value less than this $k_{\rm c}^{\rm GP}$, the condensate remains stable. This value is different to the value of $k_{\rm c}^{\rm GP} = 0.627$ obtained by Carr and Castin [6] through numerical relaxation of the 3D Gross-Pitaevskii equation. However, our result is consistent with Gammal *et al.* [17] who employed numerical relaxation under a weak axial trap of $\lambda = 0.01$ (very close to the axially-homogeneous case) and obtained $k_{\rm c}^{\rm GP} = 0.676$. Furthermore, this value is in good agreement with Salasnich *et al.* [7] who analytically derived $k_{\rm c} = 2/3$ from the

nonpolynomial Gross-Pitaevskii equation.

In contrast to the adiabatic ramping method of quantifying $k_{\rm c}^{\rm GP}$, the numerical relaxation approach relies on searching for solutions to the Gross-Pitaevskii equation (by propagating in imaginary time) for increasing values of k, and locating $k_{\rm c}^{\rm GP}$ as being the point when solutions can no longer be found. This has been employed successfully to obtain the critical interaction strength for attractive condensates under 3D trapping [15, 17]. However, for BSWs close to the critical interaction strength, the local energy minimum representing the BSW solution can be so shallow (see solid line in figure 3(c)) and localised that the imaginary time method is very sensitive to the initial guess and can become ineffective unless the initial guess is practically the solution itself.

2.3. Lengthscales of the bright solitary wave

The axial and radial widths of the BSW solutions, l_z^0 and l_r^0, are shown in figure 2(b) as a function of k, from the full Gross-Pitaevskii equation (crosses) and the sech-based variational method (lines). We evaluate the axial width of the Gross-Pitaevskii equation solutions as being the lengthscale over which the axial density decreases to $\mathrm{sech}^2(1)n_0 \simeq 0.42n_0$, where n_0 is the central peak density, and the radial width as the lengthscale over which the radial density decreases to n_0/e.

The variational and full Gross-Pitaevskii equation methods give the same qualitative description. The wave is elongated in the axial direction ($l_z^0 > l_r^0$), with radial width l_r^0 remaining close to a_r while the axial width l_z^0 diverges as $k \to 0$. For increasing interaction strength, l_z approaches l_r, and at the point of collapse the BSW is approximately isotropic ($l_r^0 = l_z^0$), as noted elsewhere [6]. However, the variational method consistently overestimates the widths predicted by the Gross-Pitaevskii equation. This implies that the variational solutions have lower peak density than the Gross-Pitaevskii equation solutions and explains why they predict a higher value of $k_{\rm c}$.

2.4. BSW energetics

Consider the variational BSW solution indicated by region II in figure 1(a). We denote the energy minimum in this region by $E_{\rm min}$. In the radial direction, the local energy minimum is well-bounded due to the dominance of the radial confinement. In the axial direction, however, there is low energy path in the energy landscape which leads from the origin to large l_z, passing through the local BSW energy minimum. We have indicated this path on the energy landscape in figure 1(a) by the dashed green line. This low-energy path represents the most energetically-favourable states of the BSW at a given axial width. In figure 3(a) and (b) we show the variation of the energy along this path, plotted on different scales to highlight contrasting features. For $l_z < l_z^0$, the energy (figure 3(a)) initially increases with decreasing l_z due to the growth of the kinetic terms in equation (5). However, for even smaller l_z the negative interaction energy begins to dominate and causes the energy to decrease (and ultimately diverge to $-\infty$ as $l_z \to 0$).

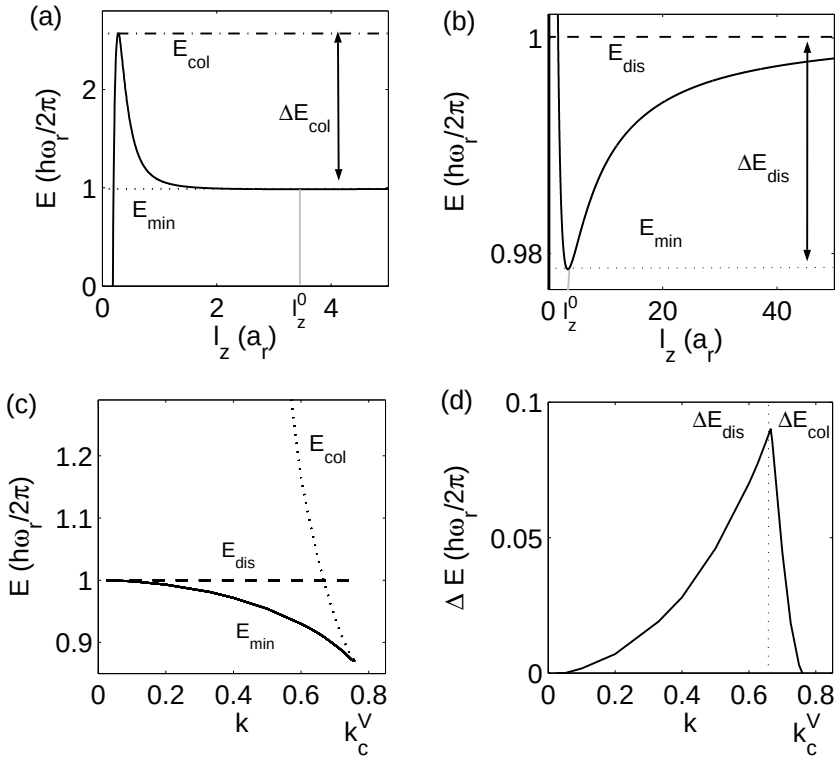

Figure 3. Energetics of the BSW (for $\lambda = 0$) according to the sech-based ansatz. (a) Energy profile along the low-energy path through the energy landscape (dashed line in figure 1(a)). The interaction strength is $k = 0.35$. The energy of the solution $E_{\rm min}$ (dotted line), the energy barrier to the collapse region $E_{\rm col}$ (dot-dashed line) and the resulting energy difference $\Delta E_{\rm col}$ are indicated. The position of the energy minimum l_z^0 is shown (grey line). (b) Same as (a) but plotted on a different scale to highlight the energy of the dispersive channel $E_{\rm dis}$ (dashed line) and the resulting energy difference $\Delta E_{\rm dis} = E_{\rm dis} - E_{\rm min}$. (c) The variation of $E_{\rm min}$ (solid line), $E_{\rm col}$ (dotted line) and $E_{\rm dis}$ (dashed line) with the interaction parameter k. (d) The excitation energy ΔE of the solution, i.e. the lower of either the collapse excitation energy $\Delta E_{\rm col}$ or dispersive excitation energy $\Delta E_{\rm dis}$.

Importantly, this gives rise to a finite energy barrier which stabilises the system against collapse. For $l_z > l_z^0$, the energy (figure 3(b)) increases weakly with l_z. This is because interaction energy in equation (5) falls off more slowly than the kinetic energy. This energy profile means that if one creates a state with $l_z > l_z^0$, then the interactions are sufficient to overcome dispersion and the state will oscillate in the energy minimum, with its length oscillating around l_z^0.

In the limit $l_z \to \infty$, the axial kinetic and interaction energy terms in equation (5) tend towards zero and the energy landscape becomes $E_{\rm sech}(l_r, l_z \to \infty) = \hbar^2/(2ml_r^2) + m\omega_r^2 l_r^2/2$, with a minimum energy $E_{\rm dis} = \hbar\omega_r$ at $l_r = a_r$. As a result we see that the low energy channel in figure 3(b) tends asymptotically towards $E_{\rm dis}$ as $l_z \to \infty$. The fact that the energy is finite at $l_z = \infty$ has important consequences. If one adds *additional* axial kinetic energy to the system, e.g. by exciting an axial breathing mode,

we can form states with higher energy than described by equation (5), i.e. states that lie above the line in figure 3(a) and (b). Importantly, if the energy of this excited state is greater than $E_{\rm dis}$ then it has sufficient energy to overcome the interactions and expand indefinitely. This means that there is a finite excitation energy $\Delta E_{\rm dis} = E_{\rm dis} - E_{\rm min}$ to induce dispersion of the BSW, as indicated in figure 3(b). We term this the *dispersive channel* (DC), as illustrated in figure 1(a).

There is another channel by which the BSW can be excited to a non-solitonic state. For axial widths less than l_z^0, there is a high-energy saddle point in the energy surface that links the local BSW energy minimum to the collapse region. We term this the *collapse channel* (CC) and have indicated it in figure 1(a). In figure 3(a) we see this feature as an energy barrier. The energy maximum has amplitude $E_{\rm col}$ and so presents an energy barrier of magnitude $\Delta E_{\rm col} = E_{\rm col} - E_{\rm min}$ against the collapse of the BSW.

In figure 3(c) we show the variation of these energies as a function of the interaction parameter k. The energy minimum $E_{\rm min}$ decreases slightly with increasing k (solid line). The energy of the dispersive channel is independent of k (dashed line). The collapse channel energy $E_{\rm col}$ (dotted line) decreases rapidly with increasing k. When the critical interaction strength $k_{\rm c}$ is reached, $\Delta E_{\rm col} = 0$ (there is no longer an energy barrier to prevent collapse), and for $k > k_{\rm c}^{\rm V}$ no variational BSW solutions exist.

These channels introduce a finite excitation energy to excite the BSW to a non-solitary state. The minimal excitation energy (for either of these channels), ΔE, characterises the stability of the BSW. This excitation energy is plotted in figure 3(d) as a function of k. For $k \lesssim 0.66$, the dispersive channel is of lowest energy, with ΔE increasing with k. If the BSW were excited in this regime it would be prone to dispersion. However, for $k \gtrsim 0.66$ the collapse channel is of lowest energy and ΔE rapidly decreases to zero as $k \to k_{\rm c}^{\rm V}$. A BSW excited in this regime will be prone to collapse. The maximum excitation energy $\Delta E \approx 0.09\hbar\omega_r$ is finite and occurs at $k \approx 0.66$. Consequently, to maximize the thermal and dynamical stability of a BSW requires tight radial confinement and $k \approx 0.66$.

According to the JILA parameters (but with $\lambda = 0$), the weak radial trapping leads to a small excitation energy $\Delta E \approx 0.08$ nK, whereas the strong radial trapping of the Rice and ENS parameters leads to a much larger value of $\Delta E \approx 3$ nK. In the experiments, following the collapse the resulting solitonic states are sufficiently dilute that it is unlikely that the system reaches thermal equilibrium within the experimental time frame. However, we can estimate the thermal energy of the system based on the temperature prior to collapse. In the JILA experiment there are initially approximately 15000 atoms in the BEC and 500 thermal atoms, corresponding to a temperature of 4.6 nK. This suggests that a BSW in the JILA system will be unstable to thermal effects, whereas the Rice and ENS systems may just support thermodynamically-stable BSWs. However, BSWs may have enhanced thermodynamic stability due to self-cooling via the radiation of hot atoms in the untrapped direction [12]. Of course, the experiments themselves featured an axial potential, unlike the $\lambda = 0$ limit considered here, and we will see in the next section that this modifies the thermodynamic stability dramatically.

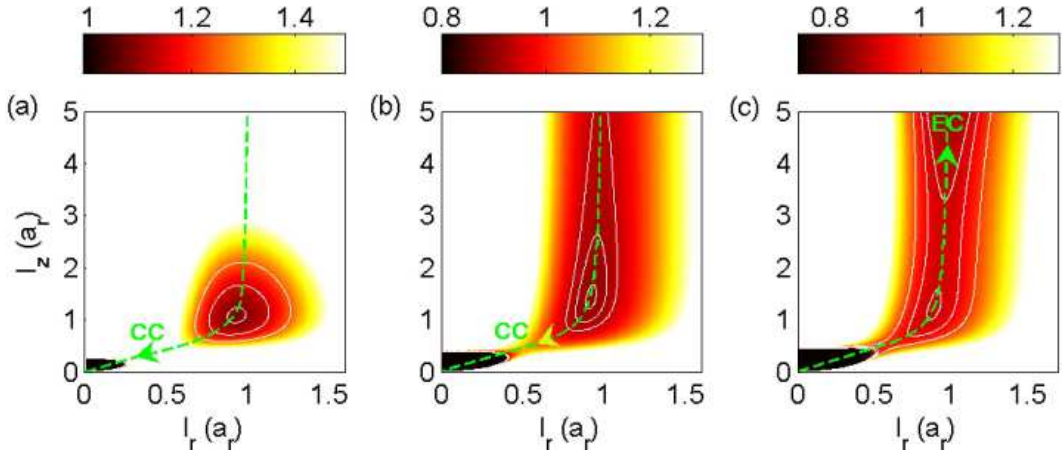

Figure 4. Energy landscapes of equation (5) for attractive BECs under the confining and expulsive axial potentials used experimentally: (a) JILA parameters with $k = 0.35$ and confining axial trapping $\lambda = 0.4$; (b) Rice parameters with $k = 0.6$ and confining axial trapping $\lambda = 0.005$. (c) ENS geometry with $k = 0.65$ and an expulsive axial potential ($\lambda^2 < 0$) with trap ratio $|\lambda| = 0.1$. Energy is presented in units of $\hbar\omega_r$ and white contours highlight the shape of the landscapes. The dashed line in each plot indicates the low energy pathway through the energy landscape, from the origin to large l_z. In (a) and (b) the preferred decay route is the collapse channel (CC) while in (c) it is the expansive channel (EC).

3. Solutions under an inhomogeneous axial potential

3.1. Confining axial potential

We now consider the condensate solutions in the presence of a confining axial potential ($\lambda^2 > 0$). In figure 4(a)-(b) we plot the energy landscapes according to equation (5) for the parameters employed in the JILA and Rice experiments. In each case, the lowest energy path through the landscape is illustrated by dashed lines. In figure 5 we plot the energy profile along the low-energy path through the energy landscape. Due to the axial confinement the $\lambda^2 l_z^2$-term in equation (5) dominates for large l_z and ultimately leads to the energy increasing with l_z. Consequently there is no dispersive channel in this system, as evident from figure 5 (dashed line). The presence of even small axial trapping therefore has a profound increase in the stability of the state. The large trap ratio of the JILA experiment ($\lambda = 0.4$) significantly modifies the energy landscape from the $\lambda = 0$ case (figure 1(a)), whereas the weak trap ratio of the Rice experiment ($\lambda = 0.005$) only has a weak effect on the energy landscape (on the lengthscales shown).

It is still possible to excite the solution out of the energy basin into the collapse region, as indicated by arrows in figure 4(a) and (b). According to the sech-based variational method, this excitation energy is $\Delta E = 1.32\hbar\omega_r \approx 1$ nK for the JILA experimental parameters and $\Delta E = 0.24\hbar\omega_r \approx 9$ nK for the Rice experimental parameters, which are of the order of the typical thermal energy of the BEC. These values are significantly larger than the $\lambda = 0$ case and indicate enhanced stability under

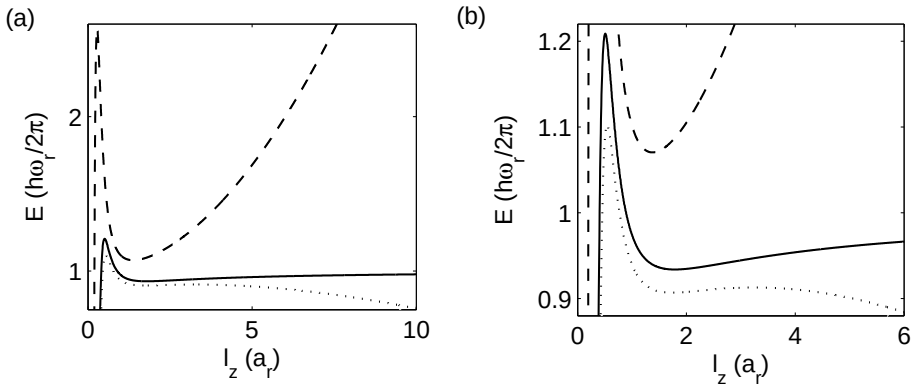

Figure 5. (a) Energy profile along the low-energy path through the energy landscape (dashed lines in figure 4(a)-(c)) for the JILA system (dashed line), Rice system (solid line) and ENS system (dotted line). (b) Same as (a) but on a different scale to highlight the small-scale features for the Rice and ENS system. Although not evident on the lengthscales shown, the energy in the Rice system tends to infinity as $l_z \to \infty$ due to the effect of the confining potential. Energy is presented in units of $\hbar\omega_r$ and each experiment features a different ω_r. Although the collapse barrier in the Rice system appears smaller than for the JILA system, it is in reality much larger due to the much larger value of ω_r employed in the Rice experiment.

an axial trap.

For an attractive BEC in a spherically-symmetric trap the critical interaction strength has been predicted to be $k_{\rm c} \approx 0.57$ by a variety of methods [16, 17, 18]. Using imaginary-time relaxation of the Gross-Pitaevskii equation, Gammal *et al.* [17] predicted $k_{\rm c}^{\rm GP}$ for various trap ratios and, for the JILA trap geometry, give excellent agreement with the experimentally measured value of $k_{\rm c}$ [10, 22]. By simulating the Gross-Pitaevskii equation under the adiabatic ramping technique we have obtained the critical interaction strength for collapse $k_{\rm c}$, with the results presented in figure 6(a) (crosses). Note that the shaded region represents stable solutions. For a confining axial potential our Gross-Pitaevskii equation results are consistent with the results of Gammal *et al.* [17] (circles). We also present the results of the sech-based variational method (dotted line) and the gaussian-based variational method (dashed line). Although these predictions give the same qualitative features, namely that $k_{\rm c}$ decreases weakly with increasing trap ratio λ, these variational methods consistently overestimate the critical interaction strength by around 20%.

In figure 6(b) we plot the axial width l_z^0 of the solutions as a function of the trap ratio λ for a fixed interaction strength of $k = 0.35$. The Gross-Pitaevskii equation (solid lines) and variational predictions (dotted and dashed lines) show good quantitative agreement. The radial widths l_r^0, shown in the inset, also show reasonable agreement.

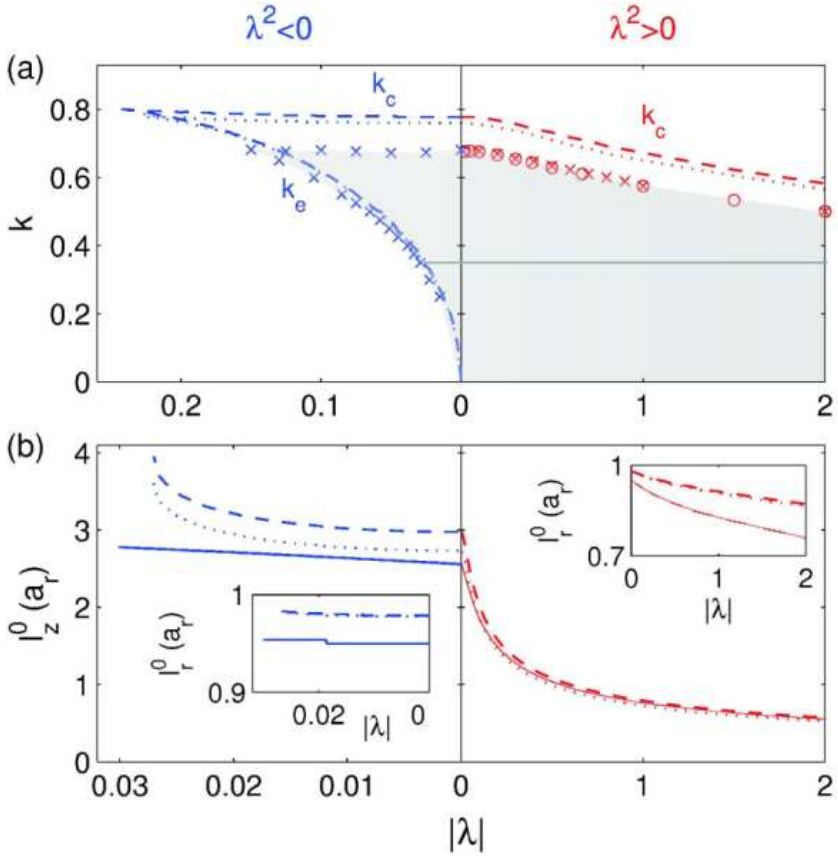

Figure 6. (a) Critical interaction strengths as a function of $|\lambda|$ for a confining potential $\lambda^2 > 0$ (red data, right-hand side of figure) and expulsive potential $\lambda^2 < 0$ (blue data,left-hand side of figure). The region of stable solutions, according to the Gross-Pitaevskii equation, is shaded. For the confining potential there is only single critical point, namely k_c for collapse, while for the expulsive trap there is additional critical point for expansion k_e. Our Gross-Pitaevskii equation results are shown by crosses, the sech-based variational method by the dotted line and the gaussian-based variational method by the dashed line. The predictions of Gammal *et al.* [17] for a confining axial trap are shown (circles). (b) Axial size of the condensate solutions as a function of $|\lambda|$ according to the Gross-Pitaevskii equation (solid line), the sech-based variational method (dotted line) and the gaussian-based variational method (dashed line). We employ an interaction strength of $k = 0.35$ such that we probe the range of solutions shown by the horizontal solid line in (a). The insets show how the radial width depends on $|\lambda|$. Note that the scale for $|\lambda|$ on the left and right sides of (a) and (b) are different.

3.2. Expulsive axial potential

The ENS experiment employed an expulsive ($\lambda^2 < 0$) trap in the axial direction [2]. This geometry leads to an additional effect whereby the wavepacket can be ripped apart by the expulsive trap [2, 6]. This occurs when k is less than a *lower* critical interaction strength for expansion k_e. The upper and lower critical interaction strengths for an expulsive trap have been mapped out using the sech-based variational method [2, 6].

The energy landscape for the ENS system is shown in figure 4(c). The energy profile

along the low-energy path through the energy landscape is shown in figure 5 (dotted line). The expulsive axial potential leads to a downward slope in the energy landscape for large l_z. In this region wavepackets will expand indefinitely. We term this the *expansive channel*, as indicated in figure 4(c). Note that we define the effect of expansion to be induced by the axial potential and so it is distinct from the effect of dispersion discussed in Section 2. The energy barrier between the solution and the expansive region *decreases* with decreasing interaction strength, such that below $k_{\rm e}$ no solutions are stable against expansion. Note that, according to the energy landscape (figure 4(c)), the minimum excitation energy is $\Delta E \approx 0.006\hbar\omega_r \approx 0.2$ nK and corresponds to excitation into the expansive region. Although this thermodynamic energy is less than the typical energy of a BEC, the expulsive trap is expected to lead to the removal of hot atoms and so may lead to anomalously low condensate temperatures.

We have calculated the critical interaction strengths for collapse $k_{\rm c}$ and expansion $k_{\rm e}$ using the Gross-Pitaevskii equation. In the former case we adiabatically ramp up k at fixed $|\lambda|$ until collapse in induced, and in the latter case we adiabatically ramp up $|\lambda|$ at fixed k until expansion is observed. In figure 6(a) (left-hand side) we plot $k_{\rm c}$ and $k_{\rm e}$ as a function of trap ratio $|\lambda|$ using the full Gross-Pitaevskii equation (crosses), and the sech-based (dotted line) and gaussian-based (dashed line) variational methods. Note that the range of trap ratios we present is an order of magnitude smaller than for the case of the confining axial potential (right-hand side of figure 6(a)). The qualitative features are that $k_{\rm c}$ (upper data) increases weakly with trap ratio $|\lambda|$, while $k_{\rm e}$ (lower data) increases sharply from zero at $|\lambda| = 0$. The region between $k_{\rm c}(|\lambda|)$ and $k_{\rm e}(|\lambda|)$ (shaded region in figure 6(a)) represents stable solutions, the region above $k_{\rm c}(|\lambda|)$ represents interaction-induced collapse, and the region below $k_{\rm e}(|\lambda|)$ represents potential-induced expansion. At some critical trap ratio $|\lambda|_{\rm c}$, $k_{\rm c} = k_{\rm e}$, and for $|\lambda| > |\lambda|_{\rm c}$ there are no stable solutions. According to the variational methods, $|\lambda|_{\rm c}^{\rm V} \approx 0.23$ while according to the Gross-Pitaevskii equation $|\lambda|_{\rm c}^{\rm GP} \approx 0.15$.

4. Dynamical multi-soliton states

In the JILA experiment [3] up to six long-lived localised 'solitons' § were observed. These wavepackets oscillated axially in a robust manner, repeatedly colliding with each other. Interestingly, the total number of atoms could greatly exceed the critical number for collapse $N_{\rm c}$ and yet the dynamics remained stable. This is because each wavepacket contained less than $N_{\rm c}$ atoms and so was individually stable to collapse, and furthermore a π-phase difference existed between adjacent wavepackets to prevent them coalescing and collapsing [6, 7, 11, 13, 23]. A π-phase difference has also been inferred to exist in the train of solitons observed in the Rice experiment [1, 7, 23]. These π-phase differences are thought to arise through the imprints of quantum fluctuations [23] or the emergence

§ The experimental system is 3D and features axial confinement, and so the wavepackets are not solitons in the strict sense. However, in this section we will follow the experimental protocol in referring to these wavepackets loosely as solitons.

of this stable configuration through repeated instabilities [11, 24]

The JILA experiment examined configurations of up to four distinct soliton structures. We will probe the stability of configurations of several coexisting solitons in the specific JILA experimental set-up, namely a ^{85}Rb BEC in a three-dimensional trap geometry $\omega_z = 2\pi \times 6.8$ Hz and $\omega_r = 2\pi \times 17.5$ Hz. Crucially we will assume a π-phase difference between adjacent solitons. A more rigorous approach to this problem would be to study excited nonlinear states of the system rather than multiple solitons, as has been performed in quasi-1D limit using Hermite functions by Michinel *et al.* [25]. Multi-soliton states with alternating phase have also been shown to be supported by the nonlinear Schrödinger equation elsewhere [26].

4.1. Generation of dynamical multi-soliton states

We impose π-phase differences to separate the attractive BEC into several distinct wavepackets, and for each configuration examine the critical number of atoms. We define the critical number for q distinct wavepackets to be $N_{\rm cq}$. We generate the $q = 1$ solutions by imaginary time propagation of the Gross-Pitaevskii equation with constant global phase and isolate the critical number $N_{\rm c1}$ as when solutions can no longer be found. In a similar manner, we form a $q = 2$ state by solving in imaginary time subject to a π-phase difference at $z = 0$, and infer the critical number $N_{\rm c2}$.

Generation of $q > 2$ states is more complicated. To form a $q = 3$ solution we employ two π-phase steps at $z = \pm L/2$, as illustrated in figure 7(a), to form three distinct regions $z \leq -L/2$, $-L/2 < z < +L/2$ and $z \geq +L/2$. Imaginary-time propagation of the Gross-Pitaevskii equation under these phase constraints can preferentially populate the central region to point of collapse. Instead we generate the $q = 3$ states dynamically, with an example shown in figure 7(c). Initially we form the ground state with constant phase and repulsive interactions. Then, in real time, the interactions are switched to attractive while the stepped phase distribution (figure 7(a)) is imprinted onto the condensate for a finite time (a time of $\Delta t = 80$ms works effectively). This forms three wavepackets with no atom transfer between them (figure 7(c)). This dynamical method of generating solitons is loosely analogous to the experimental generation of solitons. However, whereas the alternating phases arise naturally in the experiment, we must introduce them numerically.

When the phase imprinting is terminated, and providing the critical number $N_{\rm c3}$ is not exceeded, the solitons oscillate axially and repeatedly collide (figure 7(c)), as observed experimentally. The alternating phase structure prevents overlap and suppresses the collapse instability. However, the solitonic interaction excite collective modes in the solitons. When N exceeds a critical value, the system is unstable to collapse and the solitons are destroyed. This critical value depends on the lengthscale L, and so to obtain $N_{\rm c3}$ we must vary L to obtain the most stable configuration. We find that the most stable configurations arise when $L \approx 2\xi$. In order to generate a $q = 4$ state we perform a similar process by imposing three π-phase steps at $z = 0$ and

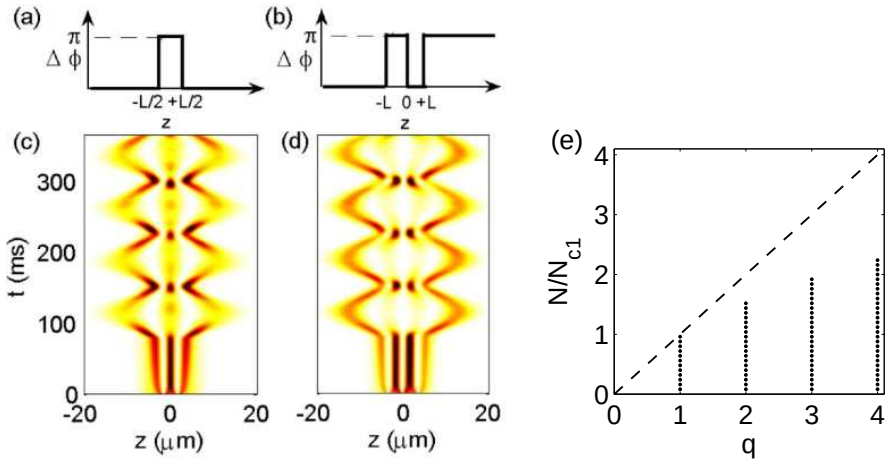

Figure 7. (a)-(b) The stepped phase profiles, with characteristic size L, used to dynamically generate $q = 3$ and $q = 4$ states. The phase profiles are enforced until $t = 80$ms. (c) Evolution of a $q = 3$ and (d) $q = 4$ state with $N = 3000$, and $L = 3.5\mu m$. Following the JILA experiment, we employ $a_s = -0.6$ nm. The plots show the evolution of the axial density, integrated over the radial direction.(e) Stability diagram of N/N_{c1} showing stable configurations of up $q = 1, 2, 3$ and 4 states. The line (N/N_c) is plotted for comparison (dashed line).

$z = \pm L$, as illustrated in figure 7(b). Under stable parameters, four localised solitons are formed, which subsequently oscillated in the system in a stable manner. An example is shown in figure 7(d).

4.2. Stability of dynamical multi-soliton states

The stability of states with $q \leq 4$ and a fixed scattering length $a_s = -0.6$nm is shown in figure 7(e). If each soliton was independent with critical number N_{c1}, the total critical number for q solitons would be qN_{c1}. In figure 7(e) we have plotted this estimate as the ratio N/N_c (dashed line). However, the numerical data gradually deviates from this line and $N_{cq} \leq qN_{c1}$, indicating that the solitons are increasingly affected by each other as their number increases. A similar trend was predicted in the quasi-1D approach of Michinel *et al.* [25].

An important question is how many solitons are favoured to exist for a given number of atoms N. The addition of a soliton involves adding a π-phase slip to the system, which is energetically costly. We can therefore expect that the most energetically-favourable number of solitons will be the minimum number of solitons/phase slips that can support N atoms without being unstable to collapse. This data is plotted in figure 8(a) for the three scattering lengths employed in the JILA experiment. All three data sets diverge away from the ratio N/N_c as q increases. The divergence is greatest for low scattering lengths, which is related to the fact that these wavepackets are widest (since the soliton size is characterised by $\xi \propto 1/\sqrt{a_s}$) and therefore interact most with their neighbours. The region above the points represents configurations of the system which are completely

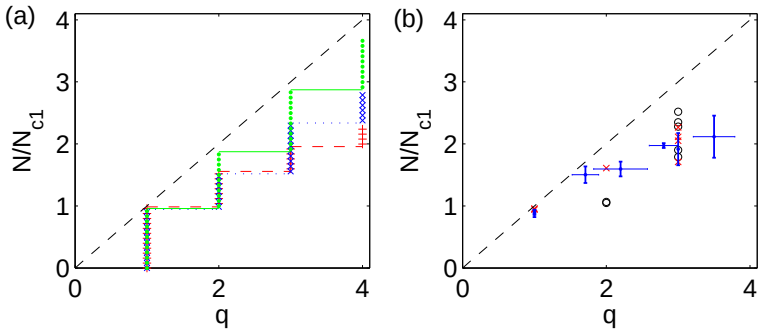

Figure 8. (a) The ratio $N/N_{\rm c1}$ versus the most stable number of solitons q (up to $q = 4$) for scattering lengths $a_{\rm s} = -0.6$nm (red pluses/dashed line), -0.77nm (blue crosses/dotted line), and -1.59nm (green circles/solid line). (b) The experimental remnant data of [3] (blue points with error bars) and the corresponding numerical data where $N = N_{\rm exp}$(black circles). Numerical data corresponding to $N = 0.9N_{\rm exp}$ is also shown (red crosses). Note that the points are for different scattering lengths.

unstable to collapse. The region below the lines in figure 8(a) also represents stable configurations of the system, but these configurations consist of a higher number of solitons/phase slips, and therefore correspond to higher energy.

4.3. Comparison with the JILA experiment

The JILA experiment [3] measured the observed number of solitons q and the total number of atoms N in each case, and the experimental data is presented in figure 8(b) (points with error bars). Note that both q and N were averaged over many observations, and generally feature an error representing the spread in their observations. Although this data shows the same trend as our numerical data in figure 8(a) (for fixed $a_{\rm s}$), it should be note here that each point corresponds to a different scattering length. We have therefore plotted the corresponding numerical results in figure 8(b). However, it is important to note the following: the number of atoms measured experimentally in the system $N_{\rm exp}$ will typically include non-condensed atoms, whereas in our analysis N describes the total number of atoms in the BEC. In other words, these experimental and theoretical parameters are not necessarily equal.

Initially we assume that all the experimentally observed atoms are in the BEC, i.e. $N = N_{\rm exp}$ (black circles in figure 8(b)). The numerical data is similar to the experimental data with most numerical points lying within the spread of the experimental observations. However for two data points the numerical data over-estimates q, e.g. where the experiment observes close to one and two solitons we predict two and three solitons, respectively. However, assuming that 10% of the atoms observed experimentally represent non-condensed atoms, i.e. $N = 0.9N_{\rm exp}$ (red crosses in figure 8(b)), we find that these two anomalous points are corrected and every numerical point is consistent with the experimental observations. This is a conservative estimate for the number of non-condensed atoms given the 'hot' state of the condensate

in the experiment.

Note that if there was zero phase difference between the solitons they would overlap upon collision, and the critical number would then be N_{c1} for $q \geq 1$.

5. Conclusions

In this paper we have considered the solutions of an attractively-interacting Bose-Einstein condensate in the mean-field limit using the full Gross-Pitaevskii equation and variational techniques. Radial confinement is assumed throughout, and in the axial direction we consider the absence of trapping and the presence of confining or expulsive harmonic potentials. In particular we evaluate the critical interaction parameter k_c for condensate collapse across the whole range of axial geometries using the full Gross-Pitaevskii equation.

We note that the variational method is not particularly sensitive to whether the sech-based or gaussian-based ansatz is used, even in the limits of zero and strong axial trapping. We find that the variational method gives good qualitative agreement with the full Gross-Pitaevskii equation, but that significant quantitative differences can exist, particularly in the important critical points for collapse and expansion.

In the absence of axial trapping, bright solitary wave solutions exist, which are self-trapped in the axial direction by the attractive interactions. According to the full solution of the Gross-Pitaevskii equation, we find that bright solitary wave solutions are stable to collapse only when the interaction parameter $k < 0.675 \pm 0.005$. Analysis of the energy 'landscapes' reveals a finite excitation energy to excite the bright solitary wave to non-solitonic states, characterised by either collapse or dispersion of the wavepacket. Unless the interaction parameter is close to the collapse condition, i.e. $k > 0.66$, the BSW will tend to decay by dispersion. The excitation energy of a bright solitary wave is proportional to the radial trap frequency, and for sufficiently weak radial trapping, the excitation energy can be less than the typical thermal energy, indicating thermodynamic instability of such states.

In the presence of either a confining or expulsive axial potential, k_c becomes dependent on the trap geometry. For the confining potential, we regain the results of Gammal *et al.* [17] and good agreement with the experimental measurement of k_c [10, 22]. Under an expulsive axial trap, there is also a *lower* critical interaction strength k_e below which the trap leads to expansion of the wavepacket. Therefore k_c and k_e define the upper and lower boundaries of a range of solutions. However, when the trap ratio $|\lambda|$ exceeds a critical value $|\lambda|_c \approx 0.15$ (based on the full Gross-Pitaevskii equation), no solutions exist for any interaction strength. Whereas for expulsive potentials and no confinement the main decay channel is dispersion, with axial confinement the only decay mechanism is collapse. Note that, for a weak expulsive potential, one can tune the system such that the energy barrier for collapse and dispersion are equal.

Finally, based on the JILA experiment [3] we have generated dynamical states of multiple 'solitons' with alternating phase. We have mapped out the critical numbers

for these states and find good agreement with the quantitative experimental data, confirming the important role of π-phase differences in systems of multiple solitons.

Acknowledgments

We thank Y. S. Kivshar and T. J. Alexander for stimulating discussions. We acknowledge financial support from the ARC (NGP/AMM), University of Melbourne (NGP/AMM), UK EPSRC (CSA) and Royal Society (SLC).

References

[1] Strecker K E *et al.* 2002 *Nature* **417** 150
[2] Khaykovich L *et al.* 2002 *Science* **296** 1290
[3] Cornish S L, Thompson S T and Wieman C E 2006 *Phys. Rev. Lett.* **96** 170401
[4] P'erez-Garcia V M, Michinel H, Cirac J I, Lewenstein M and Zoller P 1997 *Phys. Rev. A* **56** 1424
[5] Pèrez-Garcia V M, Michinel H and Herrero H 1998 *Phys. Rev. A* **57** 3837
[6] Carr L D and Castin Y 2002 *Phys. Rev. A* **66** 063602
[7] Salasnich L, Parola A and Reatto L 2002 *Phys. Rev. A* **66** 043603
[8] Nozières P and Pines D 1990 *Theory of Quantum Liquids Vol. II* (Addison-Wesley, Redwood City)
[9] Bradley C C, Sackett C A and Hulet R G 1997 *Phys. Rev. Lett.* **78** 985
[10] Roberts J L *et al.* 2001 *Phys. Rev. Lett.* **86** 4211
[11] Carr L D and Brand J 2004 *Phys. Rev. Lett.* **92** 040401
[12] Carr L D 2004 *Phys. Rev. A* **70** 033607
[13] Adhikari S K 2003 *New J. Phys.* **5** 137
Baizakov B B, Malomed B A and Salerno M 2004 *Phys. Rev. A* **70** 053613
Salasnich L 2004 *Phys. Rev. A* **70** 053617
Khaykovich L and Malomed B A 2006 *Phys. Rev. A* **74** 023607
[14] Under full 3D confinement we can define k in terms of the geometric mean of the harmonic oscillator lengths $a_{3D} = (a_z a_r^2)^{1/3} = a_r \lambda^{-1/6}$, as used elsewhere [10, 16, 17, 18, 19].
[15] Ruprecht P A, Holland M J, Burnett K and Edwards M 1995 *Phys. Rev. A* **51** 4704
[16] Houbiers M and Stoof H T C 1996 *Phys. Rev. A* **54** 5055
Dodd R J *et al.* 1996 *Phys. Rev. A* **54** 661
Akhmediev N, Das M P and Vagov A V 1999 *Int. J. Mod. Phys. B* **13** 625
Berge L, Alexander T J and Kivshar Y S 2000 *Phys. Rev. A* **62** 023607
Huepe C, Metens S, Dewel G, Borckmans P and Brachet M E 1999 *Phys. Rev. Lett.* **82** 1616
Gammal A, Frederico T and Tomio L 1999 *Phys. Rev. E* **60** 2421
[17] Gammal A, Frederico T and Tomio L 2001 *Phys. Rev. A* **64** 055602
[18] Gammal A, Tomio L and Frederico T 2002 *Phys. Rev. A* **66** 043619
[19] Yukalov V I and Yukalova E P 2005 *Phys. Rev. A* **72** 063611
[20] Pethick C J and Smith H 2001 *Bose-Einstein Condensation in Dilute Gases* (Cambridge University Press, Cambridge)
[21] Minguzzi A, Succi S, Toschi F, Tosi M and Vignolo P 2004 *Phys. Rep.* **395** 223
[22] Claussen N R *et al.* 2003 *Phys. Rev. A* **67** 060701(R)
[23] Al Khawaja U *et al.* 2002 *Phys. Rev. Lett.* **89** 200404
[24] Salasnich L, Parola A and Reatto L 2003 *Phys. Rev. Lett.* **91** 080405
[25] Michinel H, Pèrez-Garcia V M and de la Fuente R 1999 *Phys. Rev. A* **60** 1513
[26] Kivshar Y S, Alexander T J and Turitsyn S J 2001 *Phys. Lett. A* **278** 225
Carr L D, Clark C W and Reinhardt W P 2000 *Phys. Rev. A* **62** 063611